# IMINE-BASED ARCHITECTURES AT SURFACES AND INTERFACES: FROM SELF-ASSEMBLY TO DYNAMIC COVALENT CHEMISTRY IN 2D

Iwona Janica,[a,b] Violetta Patroniak,[a] Paolo Samorì,*,[c] Artur Ciesielski*,[c]

[a] Faculty of Chemistry, Adam Mickiewicz University, Umultowska 89b, 61-614 Poznań, Poland

[b] Centre for Advanced Technologies, Adam Mickiewicz University, Umultowska 89c, 61-614 Poznań, Poland

[c] Université de Strasbourg, CNRS, ISIS, 8 allée Gaspard Monge, 67000 Strasbourg, France

E-mail : samori@unistra.fr, ciesielski@unistra.fr

**ABSTRACT**

During the last two decades dynamic covalent chemistry (DCC) has emerged as an efficient and versatile strategy for the design and synthesis of complex molecular systems in solution. While early examples of supramolecularly assisted covalent synthesis at surfaces relied strongly on kinetically controlled reactions for post-assembly covalent modification, the DCC method takes advantage of the reversible nature of bond formation and allows the generation of the new covalently bonded structures under thermodynamic control. These structurally complex architectures obtained *via* DCC protocols offer a wealth of solutions and opportunities towards the generation of new complex materials holding sophisticated properties.

In this Focus Review we focus on the formation of covalently bonded imine-based discrete nanostructures, as well as one-dimensional (1D) polymers and two-dimensional (2D) covalent organic frameworks (COFs) physisorbed on solid substrates under various experimental conditions, e.g. under ultra-high vacuum (UHV) or at the solid/liquid interface. Scanning tunneling microscopy (STM) is used to gain insight, with a sub-nanometer resolution, into the structure and properties of those complex nanopatterns.

## 1.  INTRODUCTION

Supramolecular chemistry relies on the use of non-covalent forces to assemble molecular building blocks, with a sub-nanometer precision, to form superstructures and ultimately materials that display programmed chemical and physical properties.[1] Yet, the labile nature of non-covalent interactions highly affects the stability of the self-assembled structures both in liquid media and in the solid-state, thereby jeopardizing their use in technologically relevant applications. In this regard, the necessity of creating molecular architectures based on chemical components that interact through more robust, yet reversible bonds, gave rise to the field of dynamic covalent chemistry (DCC).[1-2] Noteworthy, DCC shares various features with supramolecular chemistry; in particular, they both rely on reversible bonds that enable the formation of complex structures and materials under thermodynamic control.[2-6] Both DCC and supramolecular chemistry are adaptable and modular because they allow for the selection and exchange of molecular components. On the other hand, there are some major differences between these two types of reversible chemical approaches. The equilibration processes are much faster in supramolecular systems when compared to DCC ones, because in the latter the covalent bonds need to be broken and reformed. Furthermore, DCC allows generation of structures, which are by nature more durable than the structures produced by supramolecular chemistry. For these reasons DCC is emerging as a versatile and efficient approach for the design and synthesis of complex molecular structures, which are chemically and mechanically stable.[1, 7-9]

In DCC both internal and external factors such as concentration, temperature, pressure or presence of impurities, can have a significant effect on the equilibrium and distribution of products, even after the formation of the targeted product. This variable range of parameters allows designing and creating compounds, which can adjust to the environment.[10]

While classical covalent chemistry operates under kinetic control, the DCC approach takes advantage of the reversible nature of bond formation to generate new covalent structures under thermodynamic control.[11] In particular, DCC includes the chemistry of disulfide,[12-13] acetal[14-15] and ester,[16-17] oxime,[18] boroxine,[19-20] alkynes[21] and imines[22-29] to allow the generation of new covalent structures. Chemical groups that include a C=N or carbonyl units, such as imines, esters or amides, are of particular interest since they can undergo disconnection/reconnection cycles (e.g. trans reactions like esterification, imination and amidation). Especially, the reversible nature of imine bonds makes them attractive for being used in DCC, because the (carbonyl + amine) condensation into imine-type compounds usually takes place under mild conditions.[2-5, 30-32] It is now well established that imines can participate to three types of equilibrium-controlled reactions: *i*) hydrolysis - the

imine reverts back to the precursors, i.e. amine- and carbonyl- containing compounds; *ii*) transamination - upon introduction of a second amine (or carbonyl), the original imine undergoes an exchange of the amine residue to give a new imine; *iii*) imine–imine exchange – upon introduction of a second imine, the two imines can undergo a reaction whereby the amine components are exchanged.[33] Noteworthy, dynamic exchanges that involve the C=N bonds in imines, hydrazones and oximes are the most widely used DCC reactions. They have been applied to the syntheses of complex two-dimensional (2D) and three-dimensional (3D) systems such as covalent organic frameworks (COFs).[34]

The need to explore matter at the sub-molecular scale in the direct space has made scanning tunneling microscopy (STM) a widely employed and extremely powerful tool to study surfaces and interfaces.[35-45] Since its invention in 1982,[46] STM is commonly exploited to bestow electronic and chemical information onto supramolecular assemblies.[35-36, 47-50] The sub-nanometer resolution that can be achieved with STM makes it possible to acquire thorough insight into intra- and intermolecular molecular interactions; thus, it is an essential tool to assist in the design of (supra)molecular modules that undergo controlled assembly at solid substrates under various experimental conditions (concentration,[51] temperature[52] and pressure[53]) to generate the superstructures. Beyond the mere imagining of the physisorbed monolayers,[54-55] recent studies have demonstrated that STM is the most powerful tool to study physical and chemical properties of nanostructures *via*, e.g. molecule manipulation,[56-60] monitoring of molecular dynamics[43, 61] and surface chirality,[62] etc.

Currently, STM investigations of molecular adsorption can be achieved under various environmental conditions, e.g., under ultra-high vacuum (UHV), at the solid/liquid and at the solid/air interfaces. The latter represents a remarkably versatile environment for the self-assembly of molecular building blocks, and offers numerous advantages, if compared to STM operating under UHV. In particular, the molecules physisorbed at the solid-liquid interface are at the thermodynamic equilibrium with those solvated in the 3D supernatant solution. As a result, dynamic adsorption/desorption processes take place, thereby fostering self-healing of defects in self-assembled monolayers.[63] Moreover, STM operating at the solid/liquid interface offers the possibility of screening the changes in the structural motifs of molecular monolayers upon exposure to external physical or chemical stimuli, e.g., by varying the temperature,[64] irradiation with UV light,[65] coordination of metallic centers to organic ligands,[66-68] or by changing the pH.[69] Noteworthy, such modifications can occur in a reversible manner, while under UHV molecular re-organizations are mostly irreversible.

Herein, we will discuss the engineering of one-dimensional (1D) and two-dimensional (2D) imine-based supramolecular structures through the self-association of aldehydes and amines on atomically flat, solid substrates, as explored by STM operating at the solid/liquid interface and under UHV. In the first section (2.1), we focus on the recent examples of

discrete imine-based assemblies. Further on, in (2.2) we give a perspective into the strategies employed for *bottom-up* fabrication of 1D polymers. In the final section (2.3) we address the on-surface *in situ* Schiff-base condensation between aldehydes and amines as a path towards extended 2D imine-based COFs.

## 2. DISCUSION

Recently, on-surfaces covalent chemistry has attracted a great attention and it is now being exploited to direct the topology of the resulted nanostructures. On the one hand, the on-surface covalent chemistry has unique features from the viewpoint of fundamental surface science. At a first glance, the chemical reactions taking place on the surface appear quite similar to the corresponding bulk reaction, since they are based on the same reaction precursors and reaction process. Yet, during the reaction the substrate surface is not only a passive element, i.e. a solid support, but it can play an active role. For example, if one compares the same condensation reaction taking place at the solid/liquid interface or in solution, the former is usually faster, due to higher local concentration at the solid/liquid interface compared to the one existing in the 3D solution. In other words, confinement in quasi-2D eases the reaction by decreasing activation barrier.[70] For example, the formation of the same quantity of the condensation product at the solid/liquid interface can be as $10^4$ times faster than in solution.[71] Furthermore, the on-surface synthesis represents a facile route towards novel nanostructures that cannot be generated by other methods. For example, surface can be used as template to support the synthesis of 2D polymers, which cannot be obtained from classical solution-phase route.[72]

General method towards synthesis of imines at the solid/liquid and solid/gas interface relies either on co-deposition of a mixture of the monomers or on the formation of monolayer of aldehyde and subsequent addition of amine on the top of pre-existing aldehyde assembly. The organic solvents employed for STM measurements need to combine certain characteristics: *i*) be a good solvent for the compound under study, *ii*) have a low affinity for the substrate, i.e., have a low tendency to physisorb onto its surface, *iii*) possess a low vapour pressure, enabling measurements to be carried out with the tip immersed inside one drop of solution (ca. 5–20 μL) without the necessity of employing a sealed fluid cell, and *iv*) be electrochemically inert under experimental conditions. In most cases, aldehydes and amines are dissolved in 1-phenyloctane or in octanoic acid. Rarely, small amount of pyridine is employed in order to increase the solubility of amines.[71] Noteworthy, the surface mobility and intermolecular interactions between monomers have similar impact on the on-surface polymerization carried out in ultra-high vacuum (UHV) and at the solid/liquid interface. An interplay of the adsorption processes and DCC leads to a shift in the equilibrium thus favoring the formation of the imines with higher affinity towards HOPG, which indicates a

surface-induced selection of the imines that presents the thermodynamically most-stable physisorption.

## 2.1. DISCRETE ASSEMBLIES – IMINES

Initially, surface-supported syntheses of imines have been carried out on single-crystal metallic substrates. For example, the on-surface condensation between dialdehyde **11** (Figure 1) and amine **18** (Figure 2) could be accomplished under UHV. Weigelt and co-workers firstly deposited **11** on the Au(111) and then exposed the self-assembled monolayer to the vapors of octylamine (**18**) ($1–5\times10^{-8}$ mbar).[73] The dialdehyde **11** physisorbs with its backbone oriented parallel to the basal plane of the substrate and forms well-ordered structures (Figure 3b); with the bright protrusions at the extremities of the molecules can be ascribed to the *tert*-butyl groups of **11**. On the other hand, the amine **18** forms a densely packed lamellar structure as displayed in Figure 3c.
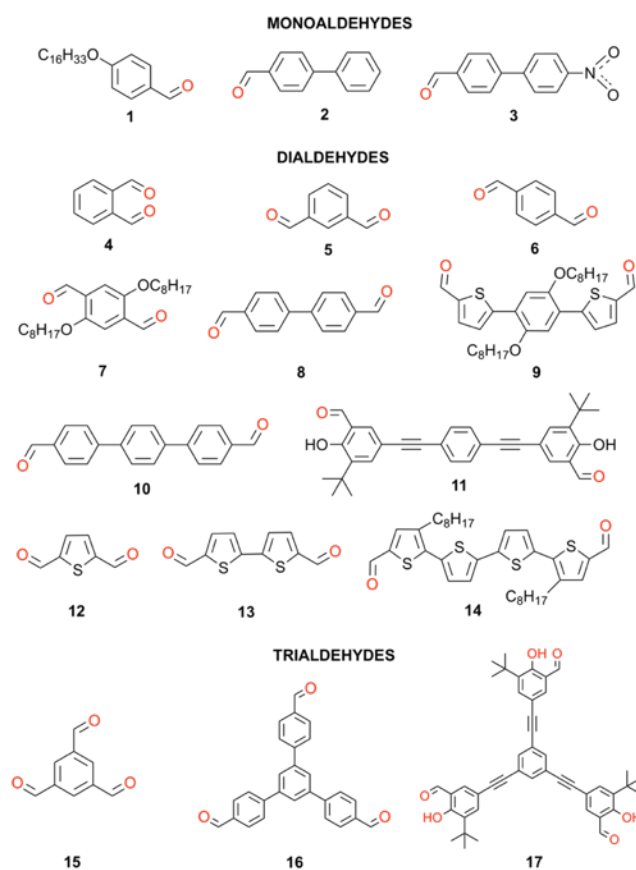


**Figure 1.** Chemical structure of investigated aldehydes: **Monoaldehydes**: (**1**) 4-(hexadecyloxy)benzaldehyde; (**2**) 4-biphenylcarboxaldehyde; (**3**) 4'-nitro[1,1'-biphenyl]-4-carbaldehyde; **Dialdehydydes**: (**4**) phthalaldehyde; (**5**) isophthalaldehyde; (**6**) terephthalaldehyde; (**7**) 2,5-bis(octyloxy)terephthalaldehyde; (**8**) [1,1'-biphenyl]-4,4'-dicarbaldehyde; (**9**) 5,5'-(2,5-bis(octyloxy)-1,4-phenylene)bis(thiophene-2-carbaldehyde); (**10**) [1,1'4'-terphenyl]-4,4''-dicarbaldehyde; (**11**) 5,5'-(1,4-phenylenebis(ethyne-2,1-diyl))bis(3-(tert-butyl)-2-hydroxybenzaldehyde); (**12**) 2,5-thiophenedicarboxaldehyde; (**13**) [2,2'-bithiophene]-5,5'-dicarbaldehyde; (**14**) 3,3'''-dioctyl-[2,2':5',2'':5'',2'''-quaterthiophene]-5,5'''-dicarbaldehyde; **Trialdehydes**: (**15**) 1,3,5-triformylbenzene; (**16**) 1,3,5-tris(4-formylphenyl)benzene; (**17**) 1,3,5-tris[(5-tert-butyl-3-formyl-4-hydroxyphenyl)ethynyl]benzene.
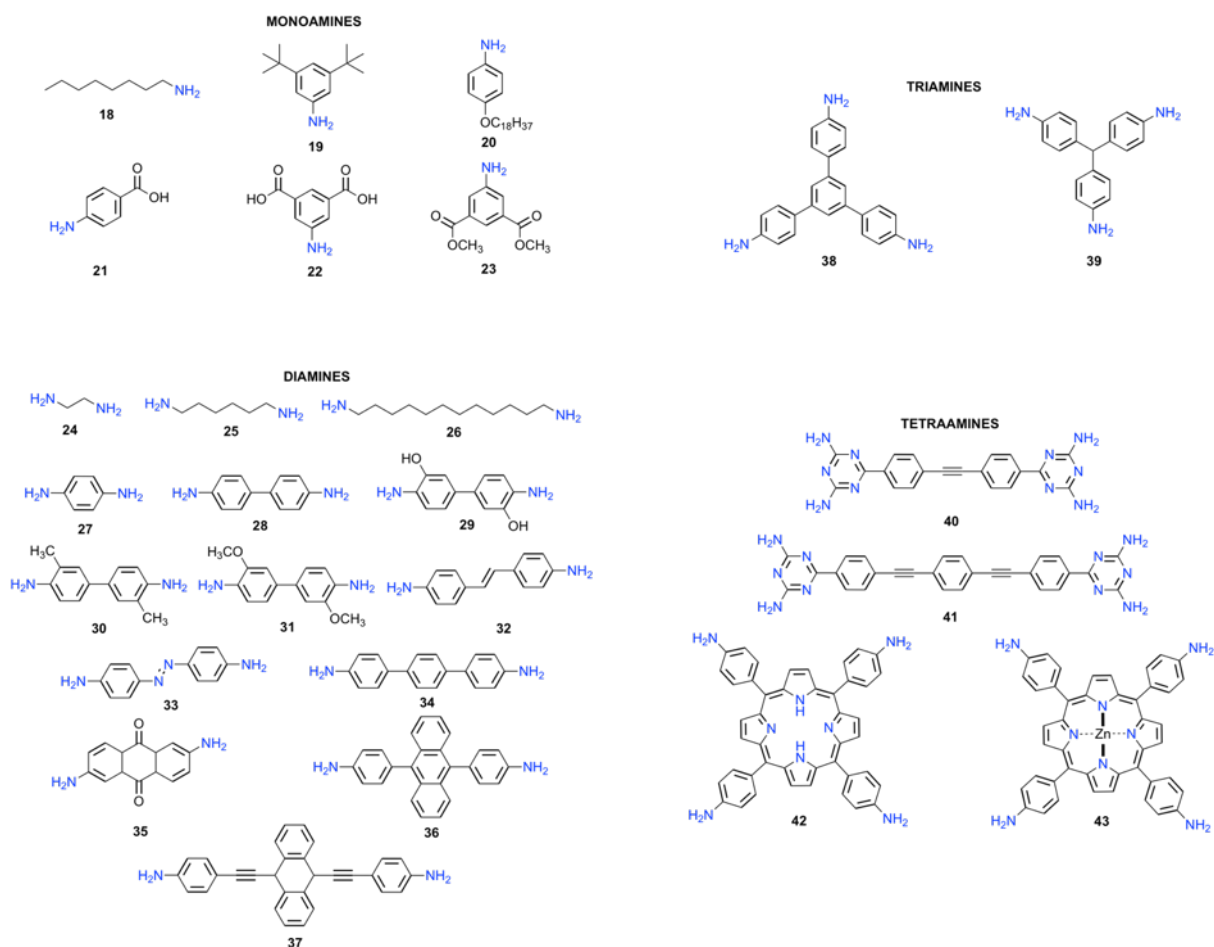
**Figure 2.** Chemical structure of investigated amines: **Monoamines**: (**18**) octylamine; (**19**) 3,5-di-tert-butylaniline; (**20**) 4-(octadecyloxy)anilinę; (**21**) 4-aminobenzoic acid; (**22**) 5-aminoisophthalic acid; (**23**) dimethyl 5-aminoisophthalate; **Diamines**: (**24**) 1,2-diaminoethane; (**25**) 1,6-diaminohexane; (**26**) 1,12-diaminododecane; (**27**) p-phenylenediamine; (**28**) benzidine; (**29**) 3,3'-dihydroxybenzidine; (**30**) o-tolidine; (**31**) 3,3'-dimethoxybiphenyl-4,4'-diamine; (**32**) 4,4'-diaminostilbene; (**33**) 4,4'-azodianiline; (**34**) 4,4''-diamino-p-terphenyl; (**35**) 2,6-diaminoanthraquinone; (**36**) 9,10-bis(p-aminophenylethynyl)anthracene; (**37**) 4,4'-((9,10-dihydroanthracene-9,10-diyl)bis(ethyne-2,1-diyl))dianiline. **Triamines**: (**38**) tris(4-aminophenyl)benzene; (**39**) 4,4',4''-methylidyne(trianiline). **Tetraamines**: (**40**) 6,6'-(ethyne-1,2-diylbis(4,1-phenylene))bis(1,3,5-triazine-2,4-diamine); (**41**) 6,6'-((1,4-phenylenebis(ethyne-2,1-diyl))bis(4,1-phenylene))bis(1,3,5-triazine-2,4-diamine); (**43**) 5,10,15,20-meso-tetra(4-aminophenyl)porphyrin; (**43**) 5,10,15,20-meso-tetra(4-aminophenyl)porphyrin Zn(II).

Upon condensation of the two components, highly ordered **18₂11** structures appear on Au(111) surface (Figure 3d and 3e). The protrusions in the STM images associated with the *tert*-butyl groups form parallel rows with the aromatic backbone visible between two bright protrusions belonging to neighboring rows. Alkyl chains from adjacent molecules align pair wise, similarly to the lamellar motif observed for the structure of **18**. In order to confirm these results, the bis-imine was synthesized *ex situ* in solution and subsequently evaporated onto an Au(111) surface and kept at the temperature of ca. 120 K (to avoid thermally activated surface reaction): the obtained structures were identical as those resulting from the *in situ* reactions.
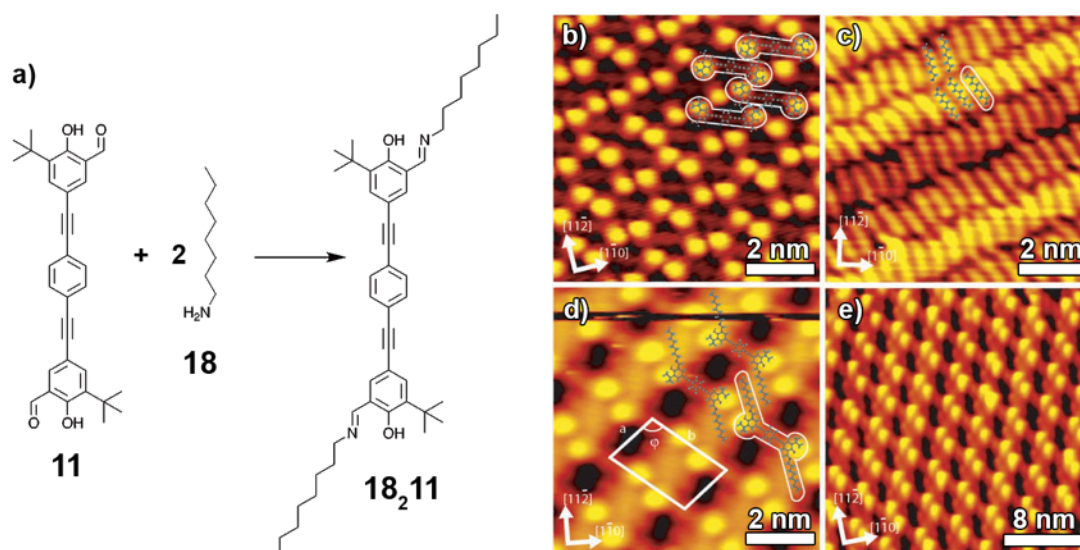
7

**Figure 3.** (a) Schematic representation of condensation reaction of aldehyde **11** with amine **18** on a Au(111) surface. STM images of (b) self-assembled island formed by the dialdehyde **11**; (c) lamellar structure formed by **18**; (d) self-assembled structure formed by the bis-imine **18₂11** prepared *in situ* at room temperature. The unit cell of the structure is indicated; (e) large ordered domain formed by the bis-imine prepared *in situ*. Imaging conditions: (b) $I_t$ = -0.77 nA, $V_t$ = -1.0 V; (c) $I_t$ = 0.41 nA, $V_t$ = +2.0 V; (d) $I_t$ = 0.27 nA, $V_t$ = +1.9 V; (e) $I_t$ = -0.42 nA, $V_t$ = -2.2 V, bar size 4 nm. Reproduced from Ref.,[73] with permissions of Wiley.

Nevertheless, due to high reversibility, mild reaction conditions and possibility to control Schiff-base reaction by various external stimuli, e.g. concentration or temperature, the solid/liquid interface has appeared superior over UHV in the last decade, as it offers a particularly interesting environment to perform condensation reactions and their *in situ* investigation by STM.

In 2014, some of us have performed a sub-molecularly resolved STM mapping of the surface-mediated reversible exchange processes of aliphatic bis-imines occurring at the solid/liquid interface on HOPG surface.[71] We have focused our attention on the condensation of 4-(hexadecyloxy)benzaldehyde (**1**) with three α,ω-diamines of different length, i.e. 1,2-diaminoethene (**24**), 1,6-diaminohexane (**25**) and 1,12-diaminododecane (**26**). Within such a work, we have reported for the first time on the STM studies on the constitutional covalent (reversible) dynamic processes of bis-transimination, i.e. diamine exchange on the bis-imines, as illustrated on Figure 4. In order to fully explore the reversible nature of imine bonds, and to gain insight into the bis-transimination processes of bis-imine molecules, successive *in situ* imination/bis-transimination cycles were performed. Upon addition of **24** on top of a pre-existing monolayer of **1** (Fig. 4a), the **1₂24** motif was obtained (Fig. 4b). Upon subsequent addition of **25** solution, the **1₂24** monolayer was transformed into an **1₂25** structure (Fig. 4c). Finally, the addition of a drop of **26** resulted in the formation of **1₂26** 2D pattern (Fig. 4d). Interestingly, the rate of the bis-transimination processes and the formation of the new monolayer structures depends on the length of diamine molecule, e.g. **1₂24** monolayers transform into **1₂25** after ca. 3 min, whereas **1₂26** monolayers are formed

after ca. 1 min after addition of **26** solution on top of **1$_2$25** structure. This observation was associated to different adsorption energies of bis-imines on HOPG surface, which increase significantly with the length of diamine linker: 33.6 kcal mol$^{-1}$, 59.3 kcal mol$^{-1}$, 71.8 kcal mol$^{-1}$ and 81.3 kcal mol$^{-1}$ for **1**, **1$_2$24**, **1$_2$25** and **1$_2$26**, respectively.
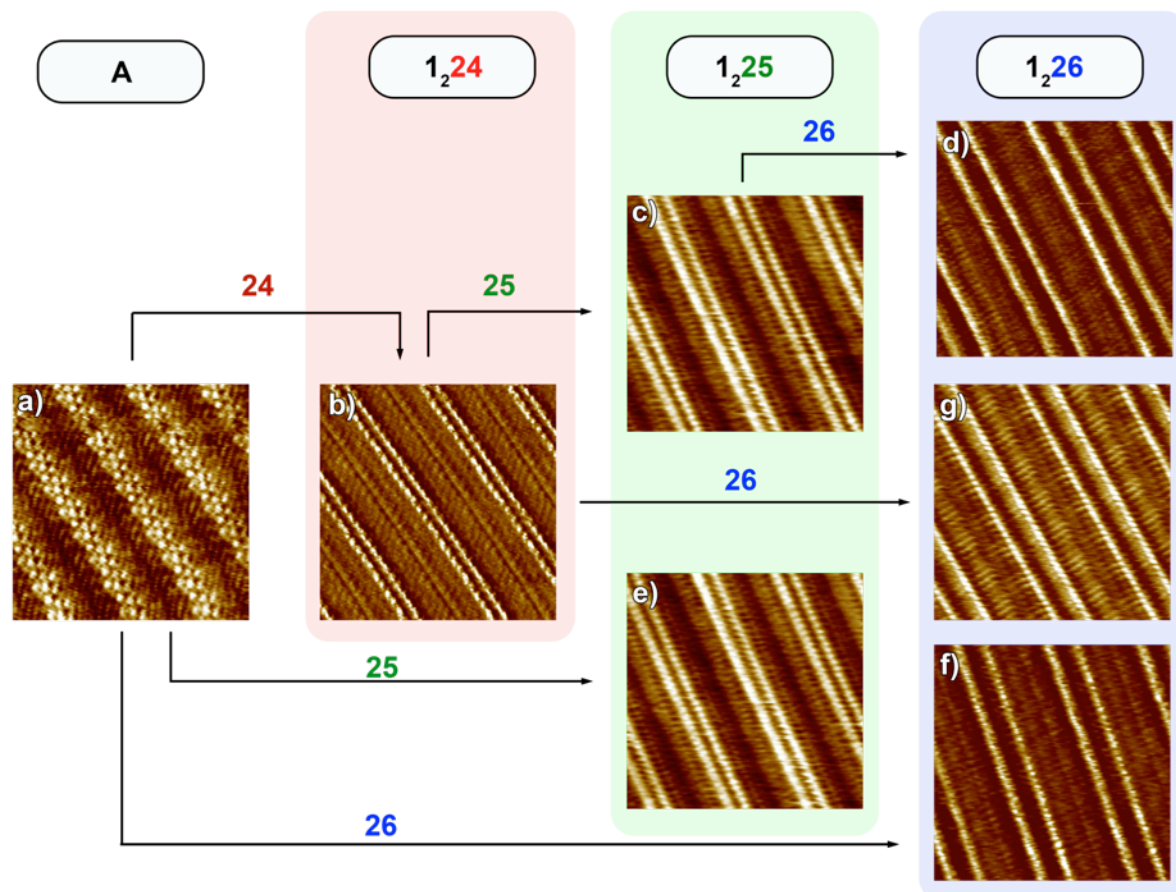


**Figure 4.** STM representative images of *in situ* condensation/bis-transimination processes. (a) the monolayer of **1**; (b) **1$_2$24** motif obtained upon *in situ* addition of **24** on top of a pre-existing monolayer of **1**; (c) On the subsequent addition of **25** solution, the **1$_2$24** monolayer was transformed into an **1$_2$25** structure; (d) the addition of a drop of **26** solution resulted in the formation of an **1$_2$26** pattern. (e) Monolayers of **1$_2$25** and (f) **1$_2$26** can be obtained by depositing a drop of **25** and **26** on top of pre-existing monolayers of **1**. (g) Bis-transimination of **1$_2$24** with **26** resulted in the formation of **1$_2$26** monolayers. Tunnelling parameters: $I_t$ = 10–15 pA, $V_t$ = 400–600 mV. The size of the STM images (a–g) is 18 nm × 18 nm. Reproduced from Ref.,[71] with permissions of Springer Nature.

The on-surface condensation of trialdehyde **16** with 5-aminoisophthalic acid (**22**) at the solid/liquid interface was investigated by Li and co-workers[74] and is shown in Figure 5. The addition of **22** on top of existing layer of **16** at room temperature resulted in formation of open-network connected by hydrogen bonds between carboxylic groups of **22**. Two different cavities appear in the network. One of them is composed of six benzene rings from six tri-imines, which are connected by hydrogen bonds between the carboxylic groups, while the second type of cavity consists of two tri-imine molecules. The structural transformation of trialdehyde **16** lamellar structures to open network after addition of amine **22** was monitored

*in situ* by STM. Upon addition of amine **22** on top of trialdehyde **16**, the lamellar structures evolve towards irregular assemblies. After 12 h, defective open-network structures appear, which still exist after 24 h. To confirm the on-surface reaction, *ex situ* synthesis of tri-imine was conducted; the subsequent deposition on HOPG surface revealed the formation of the open network identical to the one obtained *via in situ* experiments.
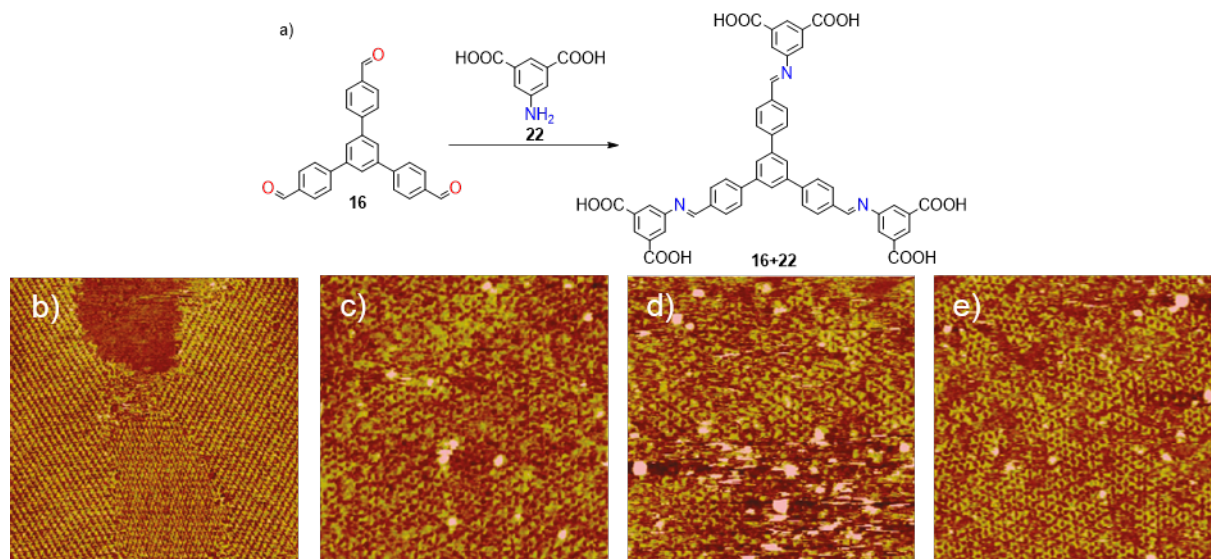


**Figure 5.** Schematic representation of condensation reaction of aldehyde **16** with amine **22** (a) and series of STM sequence images of a 70.0 nm x 70.0 nm region illustrating the structural transformation: (b) lamellar structure of aldehyde **16**; (c) irregular structure formed upon addition of amine **22** on pre-existing aldehyde **16** layer; (d) the open network after 12h and (e) 24 h. Imaging conditions: $V_{bias}$ = 935.3 mV and $I_t$ = 223.3 pA). Reproduced from Ref.,[74] with permission of American Chemical Society.

Recently, Plas and co-workers have studied the condensation reactions between aldehyde **6** with amine derivatives **19** and **20**.[75] These amino compounds were chosen due to the differences in affinity, i.e. adsorption energy, of reagents and products to HOPG, amorphous carbon and silica. A mixture of reagents **6**, **19** and **20** in the ratio 1:2:2 in 1-phenyloctane was drop-cast on to solid substrates. In the case of HOPG, it was shown that molecular self-assembly at surface is ruled by competitive adsorption. An interplay of the adsorption processes and DCC leads to a shift in the equilibrium thus favoring the formation of the imines with higher affinity towards HOPG, which indicates a surface-induced selection of the imines that presents the thermodynamically most-stable physisorption. According to STM images, as a result of the self-assembly at the solid/liquid interface, two different networks are formed. The former consists of mono-imine **6+20** with co-adsorbed small amounts of bis-imine **20$_2$6** and mixed-imine **6+19+20**, whereas the latter matches with the monolayer formed by **20**, which slowly disappears with time and is being replaced by mono-imine **6+20** network (Figure 6).
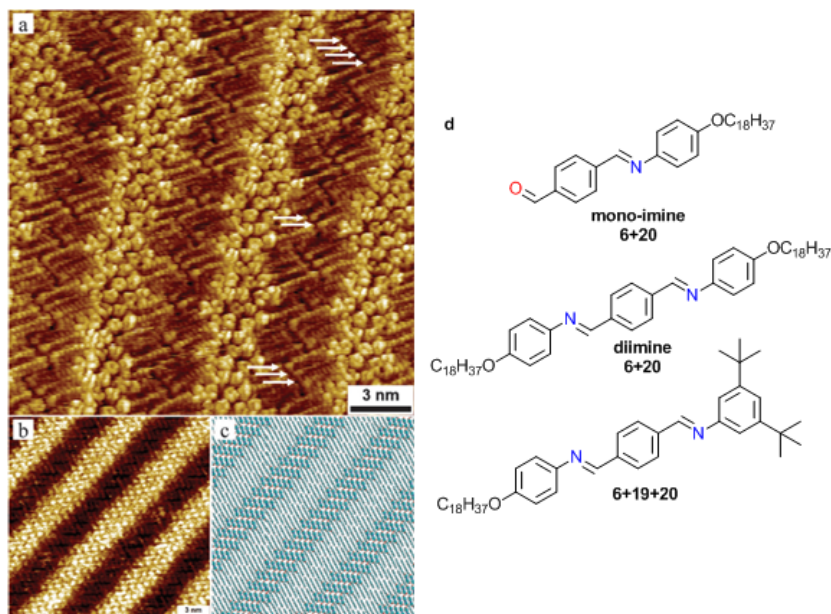
**Figure 6.** (a) STM-image of products in a monolayer formed after a mixture of **6**, **19** and **20** in 1-phenyloctane is drop-casted onto HOPG. (b) STM image of a monolayer of mono-imine **20₂6** at the 1-phenyloctane/HOPG interface and (c) the corresponding tentative molecular model; (d) chemical structures of formed products during condensation reaction of **6**, **19** and **20** at liquid/solid interface on HOPG surface. Reproduced from Ref.,[75] with permissions of Royal Society of Chemistry.

The chemical structure of the starting monomers has a great influence on the formation of imine-based nanostructures on surfaces and interfaces. For example, the achiral dialdehyde **14** and two achiral amines (**22** and **23**) could be combined to form chiral nanostructures as a result of Schiff-base condensation reactions.[76] The amines **22** and **23** were deposited on the top of an existing self-assembled monolayer of dialdehyde **14** supported on HOPG. STM investigations revealed that the adsorption of amine **22** on lamellar monolayer of dialdehyde **14** results in the formation of both clockwise and counterclockwise flower-like structures.

Generally, the monomers used for molecular physisorption at surfaces and interfaces possess a planar conformation, which enable to maximize substrate-molecule interactions thereby stabilizing the formation of self-assembled monolayer. Interestingly, Yue and co-workers showed that non-planar $C_3$-symmetrical aromatic amine molecules **39**, when combined with different aromatic aldehydes (**2**, **3**, **8** and **10**) can form porous networks on HOPG.[77] Remarkably, while the condensation between tri-amine **39** and dialdehydes should result in the generation of 2D COF, unexpected porous networks of oligomers are obtained. The Schiff-base reaction scheme between **8** and **39**, as well as the STM images of [**8₃39**]ₙ network are displayed in Figure 7. It was concluded, that the non-covalent interactions between the oligomers that stabilize the self-assembled networks disfavor the formation of 2D COFs. Within the self-assembled networks, the oligomers self-assemble in antiparallel fashion, and are stabilized *via* dipole-dipole interactions between the imine bonds and the aldehyde groups (-N=C···O=C-). Such self-assembly motif precludes the next reaction step,

11

i.e. the formation of 2D COF. Even at higher temperatures (up to 200°C), similar self-assembled structures are observed, suggesting that the self-assembly of the imine oligomer is thermodynamically favored.
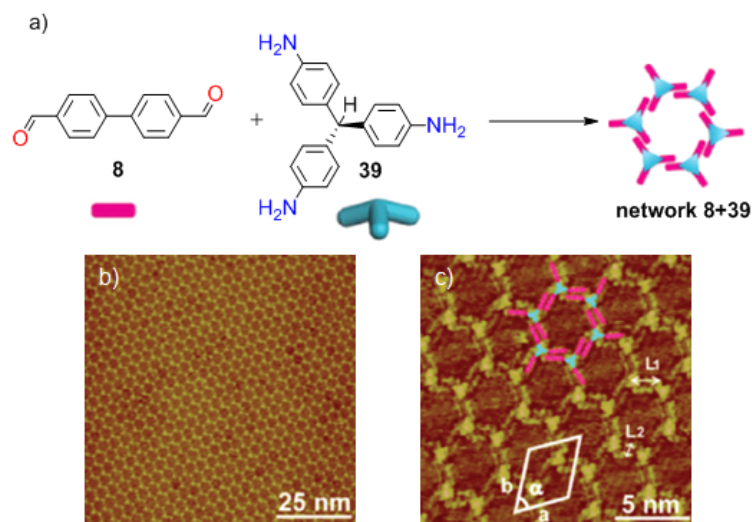


**Figure 7.** (a) The reaction between **8** and **39** results in the porous network [**8₃39**]ₙ. (b) Large-scale and (c) high-resolution STM image of network [**8₃39**]ₙ. Imaging conditions: (b) $I_t$ = 500 pA, $V_t$ = 700 mV; (c) $I_t$ = 650 pA, $V_t$ = 660 mV. Reproduced from Ref.,[77] with permissions of Royal Society of Chemistry.

Sun and co-workers exploited 2,5-bis(octyloxy)-terephthalaldehyde (**7**), 4-aminobenzoic acid (**21**) and 5-aminoisophthalic acid (**22**) as monomers for the surface-confined bis-imine formation.[78] A drop of a mixture solution of **7**, **21** and **22** was applied onto HOPG surface. When the molar ratio of monomer **7**, **21** and **22** amounted to 1:2:2, the assembly of bis-imine product **22₂7** was detected exclusively (Figure 8a), indicating that bis-imine **22₂7** is the most favorable species among all the possible products. Even when the molar ratio of monomer **21** was gradually decreased to 1:0.37:2, the bis-imine **22₂7** was still the predominant specie on HOPG. Noteworthy, at this molar ratio a second type of assembly was monitored at the domains boundaries of bis-imine **22₂7**. According to the packing mode and orientation, these shorter rods were attributed to mono-imine **22₁7**. As the molar ratio of **21** was further decreased, domains of imine **7+21** were finally visualized with the ratio of 1:0.18:2. At this molar ratio, products **7+21** and **22₂7** were found to be the dominant species, with imine **7+21** embedded as defects in domains of **22₂7** (Figure 8b). As the monomer molar ratio of **21** further decreased to 1:0.09:2, mono-imine product **7+21** finally became the exclusive specie physisorbed on HOPG (Figure 8c). Moreover, *in situ* transamination reaction was performed at the octanoic acid/HOPG interface. A deposition of an excessive amount of monomer **22** on an existing monolayer of **7+21**, resulted in the formation of the bis-imine **7+22** monolayer.[78]
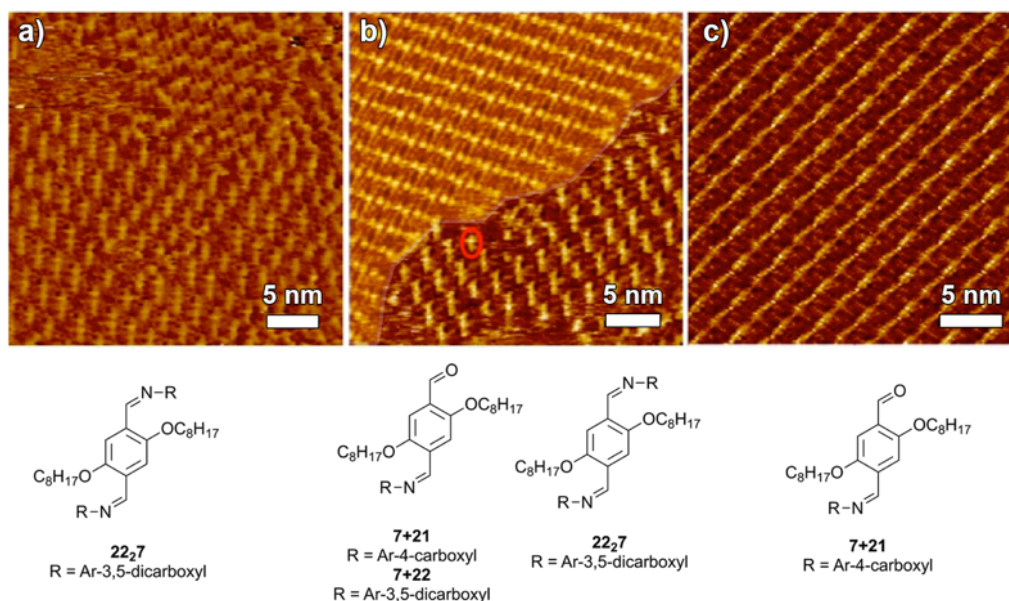
12

**Figure 8.** Typical STM images showing the evolution of the monolayer from a tri-component dynamic library of **7**, **21**, and **22**, and chemical structures of formed (bis-)imines. (a) Bis-imine **22₂7** at molar ratio of monomers 1:2:2 (b) coexistence of imine **7+21** and bis-imine **22₂7**at molar ratio 1:0.18:2 and (c) imine **7+21** at molar ratio 1:0.9:2. A molecule of imine **7+22** is highlighted by a red oval in (b). Tunneling conditions: (a) $I_t$ = 40 pA, $V_t$ = 750 mV; (b) $I_t$ = 40 pA, $V_t$ = 650 mV; (c) $I_t$ = 35 pA, $V_t$ = 700 mV. Reproduced from Ref.[78] with permissions of American Chemical Society.

In addition, coronene was employed as a template for the introduction of surface structural transformation and promotion of product selection from a tri-component mixture. Upon addition of coronene molecules onto the pre-existing monolayer of diamine **7+22**, the lamellar structure transforms intro three guest-induced architectures, featuring Kagome patterns. Yet, some of bis-imines **7+22** were also monitored on the surface.[78]

## 2.2. ONE-DIMENSIONAL (1D) POLYMERS

As a result of surface-supported condensation between dialdehydes and diamines, arrays of one-dimensional (1D) imine-based polymers have been generated. Although imines are easily formed at room temperature,[79-80] higher temperatures are sometimes required in order to obtain well-ordered and defect-free imine-based nanostructures.[81] The 1D polymers produced through surface-supported polymerization, and in particular those which contain extended π-conjugation, are appealing from a technological viewpoint as they can find use in various applications, e.g. sensors, electronic devices or heterogeneous catalysis.[22]

The nature of chemical building blocks and their concentration have significant impact on the self-assembly of 1D polymers at the solid/liquid interface. In 2015, Yu and co-workers performed the on-surface synthesis of ordered linear and *zig-zag* 1D polymers at HOPG/octanoic acid interfaces.[82] Dialdehydes **5-7** and diamines **27**, **28** and **34** were employed to form 1D polymers. In order to gain insights into different parameters of surface-mediated Schiff base coupling, three approaches were investigated: *i*) monomers were

dissolved separately in octanoic acid and then mixed prior to drop-casting onto a HOPG surface at room temperature; *ii*) after drop-casting of the mixture onto HOPG, the condensation reaction between monomers was carried out in a vacuum oven at 140°C with a base pressure of <133 Pa; *iii*) the monomers have been deposited on the top of a warm HOPG surface.

STM images of the polymers obtained *via* on-surface condensation between compound **6** and aromatic diamines **27**, **28** and **34** at the solid/liquid interface revealed the formation of highly ordered arrays of 1D polymers (Figure 9). The dense packing of the 1D polymers chains is stabilized by side-by-side van der Waals interaction between the polymeric backbones. However, as a result of co-condensation reaction between **6** and **34**, also loosely packed structure are formed, as evident in Figure 9c (marked with the red arrow). Such observation has been attributed to the repulsion between polymer chains. After changing aldehyde **6** to **7**, Schiff-base reaction between **7** with **27** and **28** resulted in highly ordered 1D polymers. The STM imaging of 1DIPs prepared *via* thermal-annealing the samples at 140°C in a vacuum oven sample after deposition did not reveal any significant differences with respect to samples prepared at the solid/liquid interface, suggesting that the reaction occurs at room temperature and further annealing does enhance the degree of polymerization. Noteworthy, for the co-condensation of **7** and **28**, the reactions carried at lower concentration ($1.6 \times 10^{-5}$ mol/L) yielded the same pattern observed at higher ones ($1.6 \times 10^{-4}$ mol/L),[80] while co-condensation of **7** with **34** at low concentration ($1.4 \times 10^{-4}$ mol/L) resulted in the formation of disordered polymers.[82] The absence of close-packed domains was ascribed to the conformational disorder brought into play by the octyl chains. Interestingly, as a result of condensation reaction of dialdehyde **5** with **27**, **28** and **34,** *zig-zag* polymers are produced.
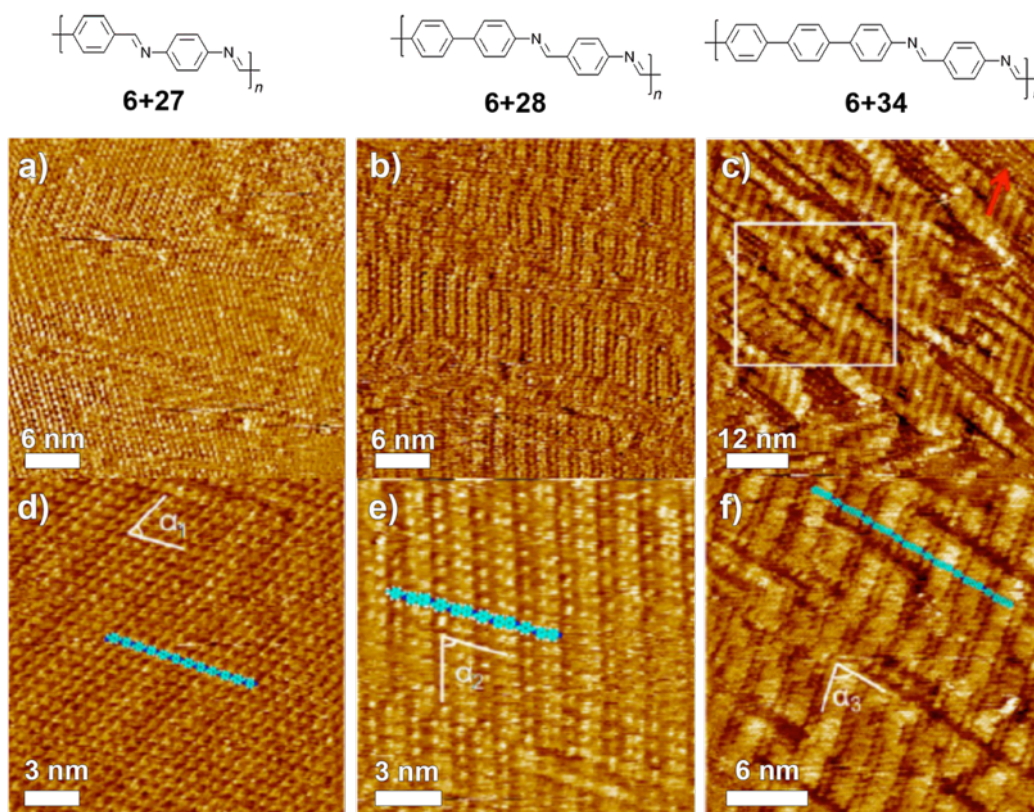
**Figure 9.** Typical (a–c) wide-area and (d–f) molecular-resolution STM images of highly ordered monolayers of linear 1D π-conjugated polymers formed at the octanoic acid/HOPG interface. Imaging conditions: (a) $I_t$ = 17 pA, $V_t$ = 0.50 V; (b) $I_t$ = 21 pA, $V_t$ = 0.56 V, (c) $I_t$ = 33 pA, $V_t$ = 0.50 V; (d) $I_t$ = 24 pA, $V_t$ = 0.63 V; (e) $I_t$ = 21 pA, $V_t$ = 0.77 V; (f) $I_t$ = 49 pA, $V_t$ = 0.50 V. Reproduced from Ref.,[82] with permissions of the American Chemical Society.

Interestingly, it has been also demonstrated that 1D polymer can be obtained from self-assembled bi-component arrays of **7** and **35**.[81] In particular, the use of quinone - an *n*-type molecule is extremely interesting from the electronic viewpoint, as it can be used to modulate the electronic properties of 1D polymers. The deposition a mixture of **7** and **35** on the HOPG surface with the molar ratio 1:1, lead to the formation of well-defined 2D networks. These networks consist of supramolecular assembly of **7** and **35**, and are laterally stabilized by the N-H⋯O hydrogen bonds between the amino and quinone or aldehyde groups. Interestingly, after 75 min, the two-dimensional network rearranges into more disordered and compact structure attributed to 1DIP. Noteworthy, similar results can be obtained by annealing existing bi-component arrays of **7** and **35** at 100°C, which accelerates the condensation between the monomers and promotes the formation of 1DIPs.

Schiff-base coupling can be controlled also by changing the pH of aqueous solutions. At low pH values most of the amino groups exist in their positively charged ammonium form ($-NH_3^+$) and they do not react with the aldehydes, while by rising the pH, the ammonium ions get deprotonated to $-NH_2$ and can react with aldehydes to form Schiff bases *via* nucleophilic addition at the aldehyde.[83] Terephthalaldehyde (**6**) and 4,4'-diaminostilbene (**32**) have been used as monomers π-conjugated 1D polymers on iodine-modified Au(111) surface.[83] The

15

pH of solutions containing monomers was adjusted with HCl or NaOH. STM investigation of the samples prepared by drop-casting the aqueous mixture of **6** and **32** at pH 2.1 and 3.6 revealed the existence of ordered 1D polymers. In aqueous solutions, at pH values below 1.5 all amino groups of **32** are protonated, i.e. they exist as ammonium ions (**32**$^{2+}$). Upon increasing pH, **32** gradually deprotonates to **32**$^0$ and above pH 5.5 **32** exist in its amino form, whereas on I/Au(111) surface, **32** behaves quite differently. At pH 1.0, the majority of **32** molecules are deprotonated to **32**$^0$, while at pH 4.0 nearly all **32** molecules are in their amino state. This was ascribed to the competition between solvation and adsorption of **32**. The solvation of deprotonated **32** on I/Au(111) is lower than **32**$^{2+}$, and the adsorption of **32**$^0$ is favored on the I/Au(111) surface and it leads to improved formation of π-conjugated 1D polymers on I/Au(111) surface. Moreover, iodine-modified Au(111) surface withdraws water molecules, which changes the equilibrium of reaction toward formation of polymers.

Tanoue and co-workers carried out Schiff-base reactions of diamines **27**, **32** and **33** with aromatic dialdehydes **4**, **5**, **6**, **12** and **13**.[84] They found that the yield of the reactions increases with the p$K_a$ of the amine, a result that can be also explained in difference of the electronic density of the amine units. The chemical structures of diamines and dialdehydes, and in particular, the substitution positions of the benzene ring have a significant influence on their reactivity during Schiff-base reactions. Based on experimental results, the reactivity of three investigated diamines has been estimated as **32** > **27** > **33**. The results of condensation between various diamines and dialdehydes are reported in Table 1.

**Table 1**. Summary of the results of Schiff-base reactions of different combinations of aromatic diamine−dialdehyde molecules in homogeneous media and onto surface ("-" – not measured). Reproduced from Ref.,[84] with permissions of American Chemical Society.

| Amine / Aldehyde | 27 (pKa = 2.9, 6.0) | | 32 (pKa = 2.9) | | 33 (pKa = 2.1, 3.9) | |
|---|---|---|---|---|---|---|
| Conditions | In homogenous media (at pH) | Monolayer on I/Au(111) (at pH) | In homogenous media (at pH) | Monolayer on I/Au(111) (at pH) | In homogenous media (at pH) | Monolayer on I/Au(111) (at pH) |
| 4 | Dispersion of dimeric product (3.5) | Disordered adlayer of dimeric product | - | - | - | - |
| 5 | Oligomeric sedimentation (3.5) | *Zig-zag* array (3.5) | - | - | Oligomeric sedimentation (6.0) | Indistinct, but layer exists (6.0) |
| 6 | Oligomeric sedimentation (3.5) | Ordered array (2.5 – 3.0) | Not reacted (2.3 – 6.0) | Ordered array (3.0) | Not reacted (4.0) Oligomeric sedimentation (6.0 – 7.5) | Ordered array (2.5) |
| 12 | Oligomeric sedimentation (3.5) | Ordered array (2.5) | Not reacted | Disordered adlayer (2.5) | Oligomeric sedimentation (6.0) | Ordered array (5.0) |
| 13 | - | Disordered array (3.0) | - | Indistinct, but layer exists (3.0) | - | - |

Reactions of **32** with dialdehydes in solution are thermodynamically favored at pH > pK$_a$ of the amine and precipitate of polycondensation products are observed with all investigated dialdehydes, except **4**. In case of **27**, which possess two distinct pK$_a$ values, i.e. pK$_{a1}$ and pK$_{a2}$, which refer to the first and second deprotonation reaction, respectively, for polyprotonic acids, the precipitate of products in homogenous aqueous solution is formed at pH values higher than pK$_{a2}$. However, between pK$_{a1}$ and pK$_{a2}$, soluble oligomeric products are obtained, while for **33**, the values of pK$_{a1}$ and pK$_{a2}$ are lower than **27** and no precipitate was observed in solution at pH region for low concentration. Remarkably, when the polycondensation reaction takes place on a hydrophobic surface such as iodine-modified Au(111), the 1D polymers can be formed at pH lower than the pK$_a$, since the reactions are accelerated by the presence of the surface, i.e. dynamic adsorption/desorption process, which confines the dimensionality of the reaction from 3D to 2D.

Recently, Yu and co-workers have systematically investigated the effect of substrate surface on the selectivity toward specific products from a multi-component dynamic covalent library, as well as the transimination occurring in 1D polymer at the solid/liquid interface.[80] In particular, an equimolar solution of **28** and **37** was deposited on a pre-existing monolayer of 1DIP generated through condensation of **7** with **28** and **7** with **37**. When a solution of **37** was

applied on top of the 1DIP **7+28**, a new 1D polymer-based pattern, i.e. **7+37** was generated. Nevertheless, after 3h, STM imaging revealed the co-existence of both polymers, i.e. **7+28** and **7+37** on the surface, thereby highlighting highly dynamic nature of 1D polymers. Noteworthy, when the transimination occurs in the middle of 1D polymer chain, a structural defect appears as a result of a mismatch in the backbone (diamine) length. Nevertheless, after annealing the sample at 100°C for 30 minutes, which promotes self-healing of 1D polymers, and in general increases the dynamics of molecules adsorbed on solid substrates, only 1D polymer **7+37** was monitored.

## 2.3. 2D COVALENT ORGANIC FRAMEWORKS

In recent years, the synthesis of covalent organic frameworks (COFs) has attracted significant attention as they can be seen as synthetic analogues of naturally occurring two-dimensional layered materials (2DLMs) such as graphene or $MoS_2$. The on-surface synthesis of 2D COFs on solid surfaces has been successfully demonstrated both under UHV[85-87] and under ambient conditions,[53, 88-89] allowing the generation of 2D polymers with single-layer thickness.[90-92] Typically, 2D or 3D COFs are obtained through formation of covalent bonds between molecular building blocks, which allows fine-tuning of their properties, and enables a precise control over composition, topology and porosity.[93-94] By choosing the suitable building blocks and appropriate synthetic protocols, it is possible to confine the dimensionality of materials to 2D.[95-97]

Similarly to graphene or other 2DLMs, 2D COFs sheets have a tendency to form layered structures in which the sheets interact *via* van der Waals forces. Such superstructures are appealing for technologically relevant applications, e.g. energy storage and charge transport. In particular, COFs based on 2D π-conjugated structures, are extremely interesting. The *bottom-up* programmability of their chemical structure opens a wealth of intriguing perspectives for the tuning of their properties with an atomic precision. In this way one can tailor 2D materials with unique electronic characteristics[98] for (photo-) electronic applications.[58, 99-102] Moreover, functionalized 2D COFs hold the potential to serve as a chelating agent, and therefore can be used in preparation of a molecular-scale membranes with well-ordered recognition sites toward metal ions, which could find applications in sensing[103] or catalysis.[99, 104-105]

Various type of 2D COFs have been obtained *via* on-surface synthesis through different types of reactions, e.g. polycondensation involving boronic acid derivatives[106-108] or Schiff bases[71, 76, 88], resulting in extended porous networks of high structural quality and large domain size.[76, 106] Nevertheless, despite the fact that the synthesis of 2D COFs on

solid substrates is very efficient, the generation of long-range ordered 2D polymers with low defect density remains extremely challenging.

First attempts of *in situ* synthesis of 2D COFs on solid substrates were conducted on single-crystal metal substrates under UHV condition. In 2008 Weigelt and co-workers have explored two various approaches towards generation of COFs. In particular, the authors studied the condensation between an aromatic trialdehyde **17** and diamine **25** on an Au (111) surface (Figure 10).[79] The first approach, which relied on the co-deposition of the monomers followed by thermal annealing above 400 K, yielded open filamentous structures, i.e. disordered fragments of 2D COF are formed (Figure 10b). In the second approach, **17** is deposited on Au (111) and treated with diamine **25** under low pressure (1-5 x $10^{-7}$ mbar) and temperature of 120-160 K, which led to the formation of multilayers. Subsequent thermal annealing (400-450 K) was used to trigger the occurrence of the condensation reaction. In particular, in the second method the sample with adsorbed trialdehyde **17** was heated to 400 K and exposed to a lower pressure (5 x $10^{-9}$ mbar) of **25**. Representative structures resulting from the second and third method are shown in Figure 10c and d, respectively.
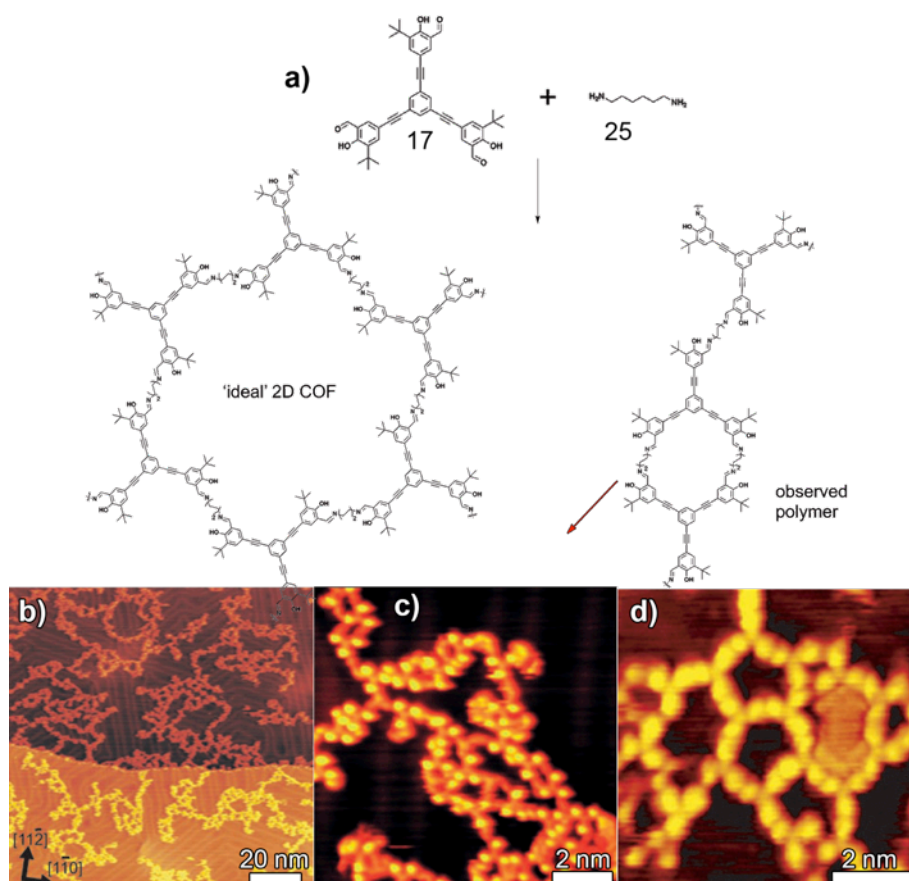


**Figure 10.** (a) Representative reaction of condensation polymerization of a trialdehyde **17** and diamine **25**. (b) Large-scale and (c, d) small scale STM images recorded after condensation reaction shows oligomeric and macrocyclic covalent structures. Imaging conditions: (b) $I_t$ = -0.66 nA, $V_t$ = -1.4 V; (c) and (d) $I_t$ = -0.35 nA, $V_t$ = -1.5 V. Reproduced from Ref.,[79] with permissions of Wiley.

As aforementioned, the condensation between the imine precursors occurring under UHV results in low coverage and the presence of topological defects. Therefore, the use of mild reaction conditions and possibility to control the condensation between the organic molecules by tuning the parameters like concentration, pH, solvent and temperature, have made the solid/liquid interface a particularly interesting environment for generation of 2D COFs, characterized by a small amount of defects and high surface coverage.[51, 71, 76, 88]

Temperature is one of the key parameters, which enables to control of 2D arrangement; it is generally believed that thermal annealing of the sample is necessary to obtain high quality 2D COFs based on imine polymers.[79, 88-89]

Triangular aldehyde **15** and linear aromatic diamines **27**, **28**, **30** and **34** were used by Xu and co-workers as precursors for the on-surface synthesis of diverse 2D COFs.[53] The synthesis of 2D COFs was carried out by: *i*) mixing **15** with one of the diamines in octanoic acid and allowing them to condensate at room temperature at the octanoic acid/HOPG or *ii*) by mixing the monomers in dimethylsulfoxide (DMSO) and polymerizing them on HOPG with moderate heating (140°C for ca. 30 min). Furthermore, low vacuum was applied to support the removal of solvent, water and unreacted monomers. This simple preparation method allowed the generation of a series of 2D COFs with tunable pore size (diameter ranging from 1.7 to 3.5 nm), which can be modulated by changing the length of diamine precursors.

The same approach has been recently exploited for tailoring imine-based 2D COFs with chemically active (–OH) or chemically passive (–OCH$_3$) groups by mixing monomer **15** with **29** or **31**.[105] Yet, the STM imaging reveled the distortion of the –OH functionalized **15+29** 2D COF, which was ascribed to the further reaction of imine with the –OH groups activated by thermal annealing (140°C).

Highly-ordered bi-component 2D COFs with honeycomb structure, can also be fabricated through self-limiting solid/vapor interface reaction method,[53, 89, 109] in which the coupling reaction is tailored in order to take place at the solid−vapor interface by introducing one precursor *via* vaporization to the surface preloaded with the other precursor. In particular, the condensation between monomers **6** and **38** or **15** and **27** was investigated by Liu and co-workers.[89] Initially, the aldehyde (**6** or **15**) is applied onto a substrate by drop-casting and then the amine (**38** or **27**) is introduced. The whole system is then sealed and placed in the reactor containing CuSO$_4$ x 5H$_2$O as thermodynamic regulation agent. By heating the reactor to 150°C, the amine precursor is brought into the vapor phase and land on the surface covered with aldehyde. Subsequently, the covalent bonds are formed at the solid−vapor interface, leading to the growth of high quality 2D COF. Noteworthy, during this process, the growth of the imine-based polymer is determined by the gas phase dosing of amine, and the redundant formation of disordered oligomers is efficiently minimized.

The porphyrin core represents a family of scaffolds possessing unique opto-electronic properties that render them interesting for various applications including catalysis[110-111] and solar cells.[112-113] The electronic, optical, and structural properties, as well as the solubility of porphyrins can be adjusted through chemical modifications with different metal centers or various substituents. The aforementioned properties in the combination with the structural features (planar geometry)[67, 114-117] make the porphyrin a superior candidate for its use for the generation of 2D COFs.[88, 109, 118]

Sun and co-workers have investigated the on-surface reaction between 5,10,15,20-meso-tetra(4-aminophenyl)porphine (**42**) and three dialdehydes, i.e. **6**, **7** and **14** on HOPG surface.[118] The synthesis of 2D COF **7+42** was conducted by applying a mixture of monomers onto the surface and subsequent annealing at 200°C for 30 minutes. The STM investigation revealed the existence of small 2D COF domains featuring a square lattice, which do not show any preferential orientation along with the major symmetry axes of graphite surface. Moreover, the presence of condensation side products, i.e. 1DIP chains, was monitored (marked white arrow in Figure 11b). In the high-resolution STM image (Figure 11c), alongside from squared structures, also rhombus architectures (black arrow) can also be observed. Such a polygon formation was attributed to the flexibility of the imine bond. The fine resolution of the STM image also enabled the detection of defects as highlighted by the blue arrow in Figure 11c, which was ascribed to the absence of one of diamine molecules in the 2D architecture.
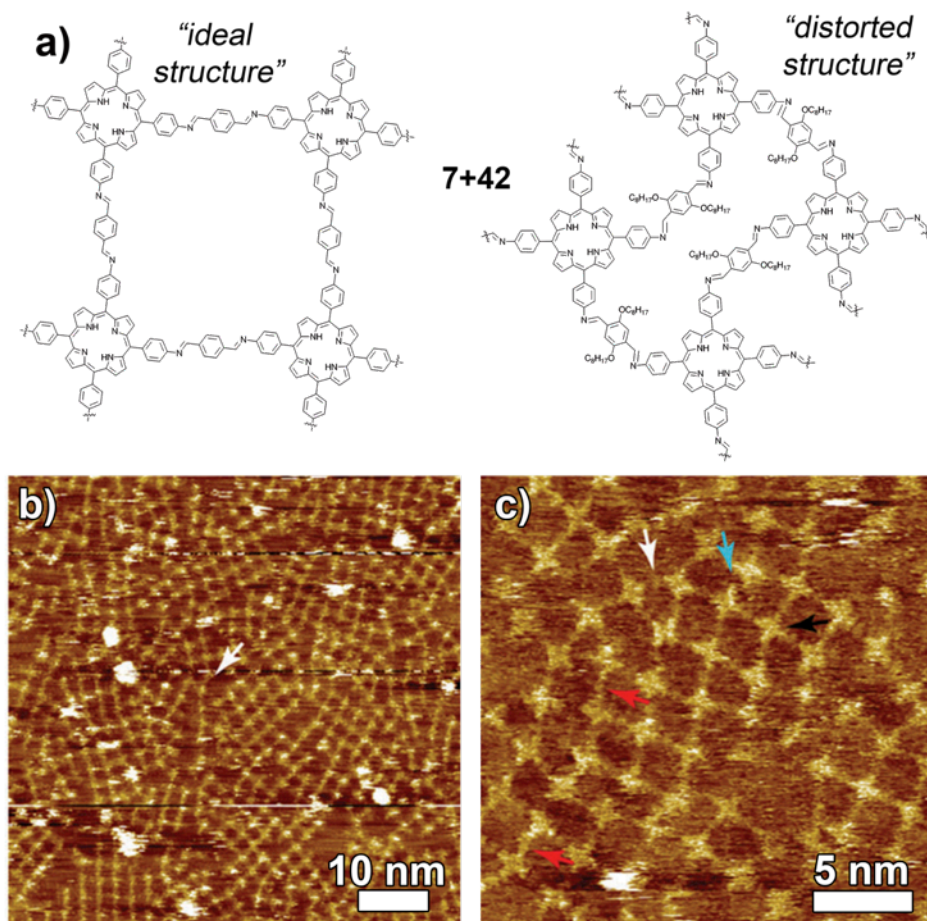
**Figure 11.** 2D COF generated via condensation between **7** and **42**. (a) Schematic representation of COF in its two various structures, i.e. squared and distorted (rhomboidal). Large scale (b) and high-resolution (c) STM images of 2D polymer of **7+42** obtained at the air-HOPG interface. The white and black arrows in (b) indicate a triangle and a deformed square, respectively, while the blue arrow points to a site where **7** is missing. The red arrows point to two **7** linker. Imaging conditions: (b) $I_t$ = 33 pA, $V_t$ = 300 mV; (c) $I_t$ = 17 pA, $V_t$ = -200 mV. Reproduced from Ref.,[118] with permissions of Royal Society of Chemistry.

According to some reports,[51, 80, 118] the most important parameters ruling the formation of 2D COFs are the concentration and the molar ratio between the molecular building blocks. The effect of the concentration on the self-assembly of supramolecular networks based on non-covalent interactions between organic molecules has been reported nearly a decade ago, and it is now well-known phenomenon in the molecular assembly at the solid/liquid interface.[119-123]

Recently, Yu *et al.* demonstrated that the same principle also applies to the on-surface formation of 2D COFs.[51] For co-condensation of the following monomers: **15+27**, **15+28**, **15+34**, **15+37**, **16+34** and **16+37**, similar concentration dependent assembling behavior was observed at the solid/liquid interface, excluding that when **37** participates in the reaction, at high concentration, where disordered amorphous polymers were observed. Representative STM images of the 2D COFs generated at room temperature are shown in Figure 12. By keeping the molar ratio between the monomers constant, i.e. aldehyde:amine = 2:3, clear influence on the optimized concentration by the size of monomers was

monitored. The optimized molar concentrations of diamines were determined as **15+27** (2.5 × $10^5$ mol $L^{-1}$) > **15+28** (1.6 × $10^5$ mol $L^{-1}$) > **15+34** (7.4 × $10^6$ mol $L^{-1}$) > **15+37** (3.5 × $10^6$ mol $L^{-1}$) and **16+34** (5.3 × $10^6$ mol $L^{-1}$) > **16+37** (2.7 × $10^6$ mol $L^{-1}$). It was concluded, that for a given aldehyde, the required concentration of amine, needed to generate 2D COF, decreases with the amine length.
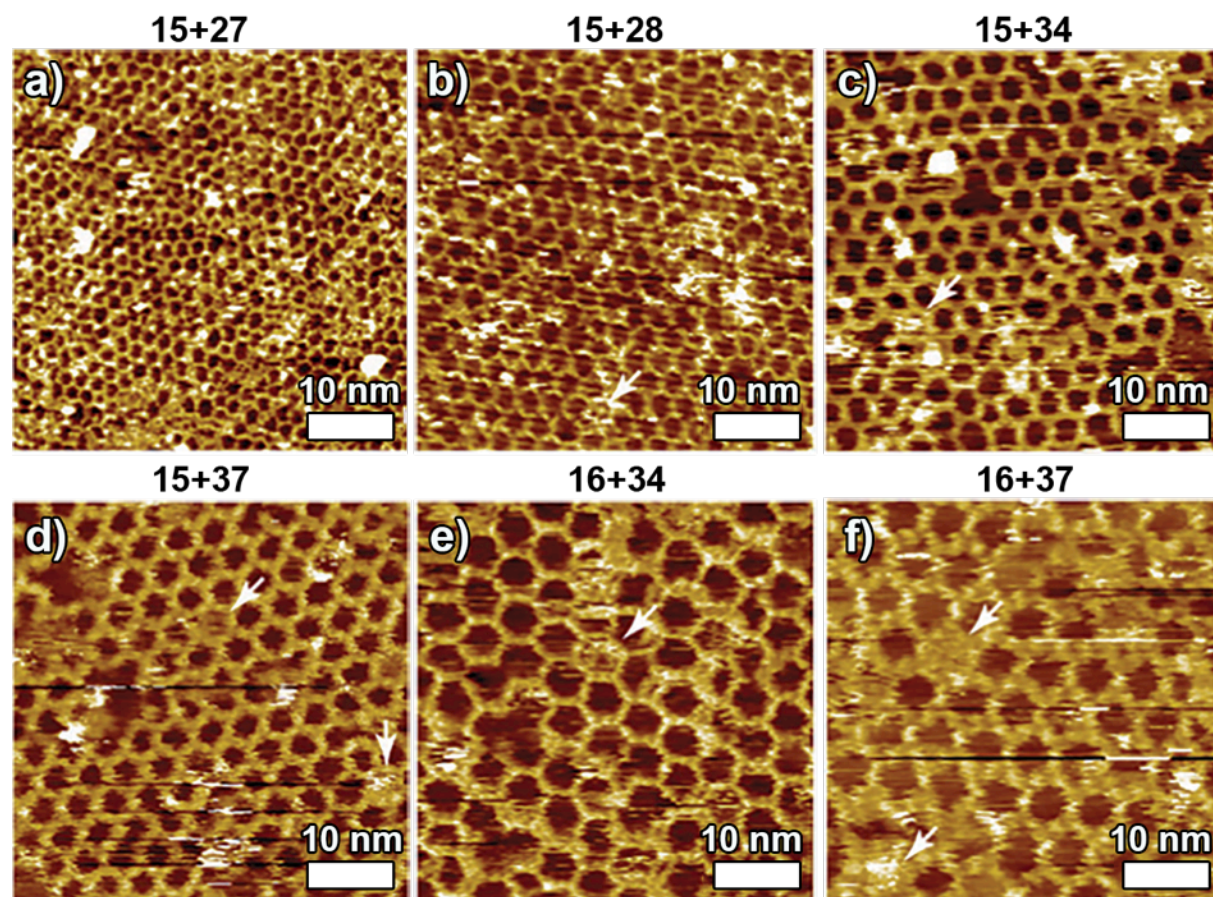


**Figure 12.** Representative STM images of 2D COFS formed at the octanoic acid/ HOPG interface. Imaging conditions: (a) $I_t$ = 36 pA, $V_t$ = 0.66 V; (b) $I_t$ = 53 pA, $V_t$ = 0.52 V; (c) $I_t$ = 30 pA, $V_t$ = 0.66 V; (d) $I_t$ = 67 pA, $V_t$ = 0.80 V; (e) $I_t$ = 30 pA, $V_t$ = 0.20 V; and (f) $I_t$ = 30 pA, $V_t$ = 1.00 V. Reproduced from Ref.,[51] with permissions of Royal Society of Chemistry.

In 2014, Xu and co-workers demonstrated a simple method for fabricating fully aromatic 2D COF, with single atomic thickness on single-layer graphene grown by chemical vapour deposition (CVD) on copper foil.[91] Benzene-1,3,5-tricarbaldehyde (**15**) and *p*-phenylene- diamine (**27**) were used as precursors. It is important to note that the properties of graphene are more complex than HOPG. The different facets, step edges, kinks, and other defects result in different molecule-substrate interactions with CVD graphene, and ultimately result in the change of its electronic properties.[124-125] An extended adlayer of π-conjugated, yet, defective structure of **15+27** COF was observed by STM upon applying a droplet of the mixture of the two precursors to the graphene surface (Figure 13b). The *in situ* formation of **15+27** COF at the solid/liquid interface can reach an equilibrium state after few

minutes. As aforementioned, the peculiar nature of the solid/liquid interface promotes self-healing of defects in self-assembled monolayers. Also in this case, self-healing of the defects, which can occur in the structure, may be observed *in situ* within ca. 1 min (Figure 13c). In Figure 13 b and c, the white arrow indicates a large open pore, which was converted into a pentagon and a hexagon. The red, violet, and blue arrows highlight the healing of the **15+27** COF surface and formation of new covalent bonds between already existing oligomers. Interestingly, the calculated band structure of **15+27** COF shows a band gap around 2 eV, indicating that the free standing **15+27** COF is a 2D organic semiconductor.
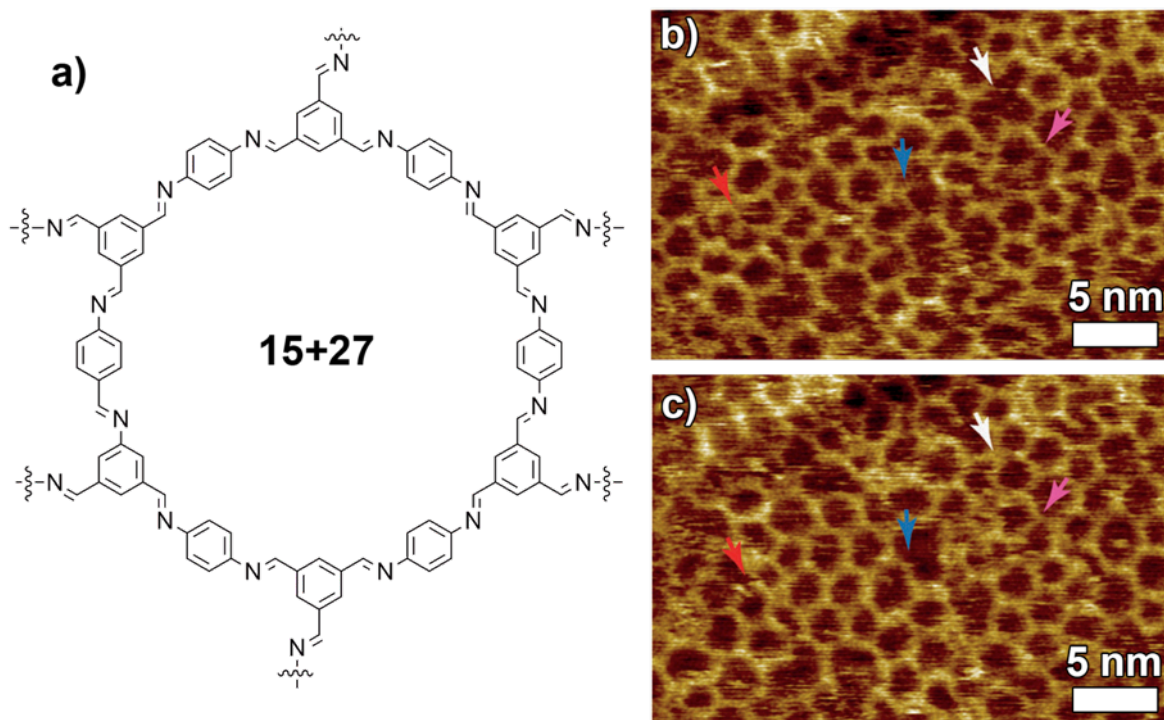


**Figure 13.** Formation of 2D COF **15+27** (a) as a result of Schiff-base reaction between trialdehyde **15** and diamine **27**. (b) and (c) two successive STM images showing the dynamic process of Schiff-base reaction of **15+27** at the octanoic acid/graphene interface. The time interval is 1.08 min. The arrows highlight the sites where noticeable changes happened. The tunneling conditions: $I_t$ = 700 pA, $V_t$ = 10 mV. (b) and (c) Reproduced from Ref.,[91] with permissions of Wiley.

## 3. CONCLUSIONS AND PERSPECTIVES

In summary, we have presented the most enlightening recent achievements in synthesis of discrete, 1D and 2D imine nanostructures *via* formation of covalent bonds between aldehydes and amines on atomically flat substrates, under various experimental conditions. Self-assembly at surfaces and interfaces is undoubtedly the most studied field towards the *bottom-up* fabrication of supramolecular structures. While many elegant imine assemblies containing 1D and 2D covalent organic frameworks have been fabricated on surfaces and interfaces, it is however clear that considerable work remains to be done. Recently, most of the on-surface synthesis of imine-based nanostructures is conducted at

the solid/liquid or gas/solid interface, due to an uncomplicated infrastructure and mild reaction conditions, which enable full control by external and internal stimuli, such as temperature, concentration, pH, solvent, etc., leading to the formation of more ordered structure, if compared to reactions performed under UHV condition. The on-surface fabrication of well-defined 1D and 2D imine-based conjugated polymers offers paths to the preparation of films with a specific thickness and a well-defined structure without the need of thermal annealing. In case of surface 2D COFs, it is possible to modify their electronic structure (by introducing substituents in desired positions with an atomic precision) or the pore size (by varying the length of the monomers). Moreover, both 1D and 2D COFs supported on solid substrates may serve as templates for the growth of 3D COFs with novel structural motifs thus functions. These results open the doors for *bottom-up* assembly of a vast array of solid-supported, designer DCC nanoarchitectures with potential application in low cost, flexible devices, electronics, solar and fuel cells, chemical and biosensors, heterocatalysis, inkjet printing, separations, nanoporous membranes, and commercial coatings.[77]

Nevertheless, as the formation of 1D and 2D COFs on solid substrates is only based on the STM imaging, further multiscale investigation (in time and space) on the chemical composition, structure and function is needed to provide unambiguous evidence of the imine formation. Functional groups that involve a C=N unit, such as imines are of special interest because they may undergo disconnection/reconnection cycles. Reversibility is an important feature of the C=N linkage. Imines are widely exploited by nature in many enzymatic processes and by organic chemists in a variety of applications, mostly due to the reversibility of the reactions under thermodynamic equilibrium. The introduction of different polar and non-polar groups to the backbone of constructed networks, which can influence pore size, polarity and reactivity may reveal the real potential of these covalent, yet, reversible type of functional materials.

## ACKNOWLEDGMENTS

## REFERENCES

[1]     S. J. Rowan, S. J. Cantrill, G. R. L. Cousins, J. K. M. Sanders, J. F. Stoddart, *Angew. Chem. Int. Ed.* **2002**, *41*, 898-952.

[2]     Y. H. Jin, C. Yu, R. J. Denman, W. Zhang, *Chem. Soc. Rev.* **2013**, *42*, 6634-6654.

[3]     J.-M. Lehn, *Chem. Eur. J.* **1999**, *5*, 2455-2463.

[4]     P. T. Corbett, J. Leclaire, L. Vial, K. R. West, J. L. Wietor, J. K. M. Sanders, S. Otto, *Chem. Rev.* **2006**, *106*, 3652-3711.

[5]     B. L. Miller, in *Dynamic Combinatorial Chemistry in Drug Discovery, Bioorganic Chemistry, and Materials Science*, John Wiley & Sons, Inc., **2009**, pp. 1-42.

[6]     W. Zhang, Y. Jin, *Dynamic Covalent Chemistry: Principles, Reactions, and Applications*, Wiley, **2017**.

[7]     J. L. Segura, M. J. Mancheno, F. Zamora, *Chem. Soc. Rev.* **2016**, *45*, 5635-5671.

[8]     C. S. Diercks, O. M. Yaghi, *Science* **2017**, *355*, 923-931.

[9]     T. Maeda, H. Otsuka, A. Takahara, *Prog. Polym. Sci.* **2009**, *34*, 581-604.

[10]    J. Elemans, *Adv. Funct. Mater.* **2016**, *26*, 8932-8951.

[11]    A. Herrmann, *Chem. Soc. Rev.* **2014**, *43*, 1899-1933.

[12]    F. Klepel, B. J. Ravoo, *Org. Biomol. Chem.* **2017**, *15*, 3840-3842.

[13]    S. P. Black, J. K. M. Sanders, A. R. Stefankiewicz, *Chem. Soc. Rev.* **2014**, *43*, 1861-1872.

[14]    B. Fuchs, A. Nelson, A. Star, J. F. Stoddart, S. B. Vidal, *Angew. Chem. Int. Ed.* **2003**, *42*, 4220-4224.

[15]    R. Cacciapaglia, S. Di Stefano, L. Mandolini, *J. Am. Chem. Soc.* **2005**, *127*, 13666-13671.

[16]    R. C. Brachvogel, M. von Delius, *Eur. J. Org. Chem.* **2016**, 3662-3670.

[17]    G. Kaiser, J. K. M. Sanders, *Chem. Commun.* **2000**, 1763-1764.

[18]    W. X. Liu, C. Zhang, H. Zhang, N. Zhao, Z. X. Yu, J. Xu, *J. Am. Chem. Soc.* **2017**, *139*, 8678-8684.

[19]    A. L. Korich, P. M. Iovine, *Dalton Trans.* **2010**, *39*, 1423-1431.

[20]    A. P. Côté, A. I. Benin, N. W. Ockwig, M. O'Keeffe, A. J. Matzger, O. M. Yaghi, *Science* **2005**, *310*, 1166-1170.

[21]    Y. Jin, Q. Wang, P. Taynton, W. Zhang, *Acc. Chem. Res.* **2014**, *47*, 1575-1586.

[22]    M. E. Belowich, J. F. Stoddart, *Chem. Soc. Rev.* **2012**, *41*, 2003-2024.

[23]    E. H. Cordes, W. P. Jencks, *J. Am. Chem. Soc.* **1962**, *84*, 832-837.

[24]    R. W. Layer, *Chem. Rev.* **1963**, *63*, 489-510.

[25]    S. Dayagi, Y. Degani, in *Carbon–Nitrogen Double Bonds* (Ed.: S. Panai), Wiley, **2010**, pp. 61-147.

[26]    L. Tauk, A. P. Schroder, G. Decher, N. Giuseppone, *Nat. Chem.* **2009**, *1*, 649-656.

[27]    R. Bonnett, in *Carbon–Nitrogen Double Bonds (1970)* (Ed.: S. Patai), Wiley, **2010**, pp. 597-662.

[28]    H. Sahabudeen, H. Qi, B. A. Glatz, D. Tranca, R. Dong, Y. Hou, T. Zhang, C. Kuttner, T. Lehnert, G. Seifert, U. Kaiser, A. Fery, Z. Zheng, X. Feng, *Nat. Commun.* **2016**, *7*, 13461.

[29]    W. Dai, F. Shao, J. Szczerbiński, R. McCaffrey, R. Zenobi, Y. Jin, A. D. Schlüter, W. Zhang, *Angew. Chem. Int. Ed.* **2016**, *55*, 213-217.

[30]    M. C. T. Fyfe, J. F. Stoddart, *Acc. Chem. Res.* **1997**, *30*, 393-401.

[31]    J.-M. Lehn, *Chem. Soc. Rev.* **2007**, *36*, 151-160.

[32]    J.-M. Lehn, in *Constitutional Dynamic Chemistry* (Ed.: M. Barboiu), Springer Berlin Heidelberg, Berlin, Heidelberg, **2012**, pp. 1-32.

[33]    M. Ciaccia, R. Cacciapaglia, P. Mencarelli, L. Mandolini, S. Di Stefano, *Chem. Sci.* **2013**, *4*, 2253-2261.

[34]    F. J. Uribe-Romo, J. R. Hunt, H. Furukawa, C. Klöck, M. O'Keeffe, O. M. Yaghi, *J. Am. Chem. Soc.* **2009**, *131*, 4570-4571.

[35]    J. P. Rabe, S. Buchholz, *Science* **1991**, *253*, 424-427.

[36] S. De Feyter, A. Gesquière, M. M. Abdel-Mottaleb, P. C. M. Grim, F. C. De Schryver, C. Meiners, M. Sieffert, S. Valiyaveettil, K. Müllen, *Acc. Chem. Res.* **2000**, *33*, 520-531.

[37] A. M. Jackson, J. W. Myerson, F. Stellacci, *Nat Mater* **2004**, *3*, 330-336.

[38] A. Cadeddu, A. Ciesielski, T. El Malah, S. Hecht, P. Samorì, *Chem. Commun.* **2011**, *47*, 10578-10580.

[39] A. Ciesielski, A. Cadeddu, C.-A. Palma, A. Gorczyński, V. Patroniak, M. Cecchini, P. Samorì, *Nanoscale* **2011**, *3*, 4125-4129.

[40] J. M. MacLeod, O. Ivasenko, D. F. Perepichka, F. Rosei, *Nanotechnology* **2007**, *18*, 424031.

[41] A. Ciesielski, G. Schaeffer, A. Petitjean, J.-M. Lehn, P. Samorì, *Angew. Chem. Int. Ed.* **2009**, *121*, 2073-2077.

[42] A. Ciesielski, L. Piot, P. Samorì, A. Jouaiti, M. W. Hosseini, *Adv. Mater.* **2009**, *21*, 1131-1136.

[43] A. Ciesielski, P. Samorì, *Nanoscale* **2011**, *3*, 1397-1410.

[44] M. E. Cañas-Ventura, W. Xiao, D. Wasserfallen, K. Müllen, H. Brune, J. V. Barth, R. Fasel, *Angew. Chem. Int. Ed.* **2007**, *46*, 1814-1818.

[45] S. Stepanow, M. Lingenfelder, A. Dmitriev, H. Spillmann, E. Delvigne, N. Lin, X. Deng, C. Cai, J. V. Barth, K. Kern, *Nat Mater* **2004**, *3*, 229-233.

[46] G. Binning, H. Rohrer, C. Gerber, E. Weibel, *Phys. Rev. Lett.* **1982**, *49*, 57-61.

[47] D. Bonifazi, S. Mohnani, A. Llanes-Pallas, *Chem. Eur. J.* **2009**, *15*, 7004-7025.

[48] A. Ciesielski, C.-A. Palma, M. Bonini, P. Samorì, *Adv. Mater.* **2010**, *22*, 3506-3520.

[49] A. Ciesielski, M. El Garah, S. Masiero, P. Samorì, *Small* **2016**, *12*, 83-95.

[50] L. Jiang, A. C. Papageorgiou, S. C. Oh, O. Saglam, J. Reichert, D. A. Duncan, Y. Q. Zhang, F. Klappenberger, Y. Y. Guo, F. Allegretti, S. More, R. Bhosale, A. Mateo-Alonso, J. V. Barth, *ACS Nano* **2016**, *10*, 1033-1041.

[51] Y. X. Yu, J. B. Lin, Y. Wang, Q. D. Zeng, S. B. Lei, *Chem. Commun.* **2016**, *52*, 6609-6612.

[52] L. X. Cheng, Y. B. Li, C. Y. Zhang, Z. L. Gong, Q. J. Fang, Y. W. Zhong, B. Tu, Q. D. Zeng, C. Wang, *ACS Appl. Mater. Interfaces* **2016**, *8*, 32004-32010.

[53] L. R. Xu, X. Zhou, Y. X. Yu, W. Q. Tian, J. Ma, S. B. Lei, *ACS Nano* **2013**, *7*, 8066-8073.

[54] *Scanning Probe Microscopies Beyond Imaging: Manipulation of Molecules and Nanostructures, Ed. P. Samorì*, WILEY-VCH Verlag GmbH & Co. KGaA, Weinheim, **2006**.

[55] P. Samorì, *J. Mater. Chem.* **2004**, *14*, 1353-1366.

[56] L. Grill, M. Dyer, L. Lafferentz, M. Persson, M. V. Peters, S. Hecht, *Nat. Nanotechnol.* **2007**, *2*, 687-691.

[57] B. Hulsken, R. Van Hameren, J. W. Gerritsen, T. Khoury, P. Thordarson, M. J. Crossley, A. E. Rowan, R. J. M. Nolte, J. A. A. W. Elemans, S. Speller, *Nat. Nanotechnol.* **2007**, *2*, 285-289.

[58] D. F. Perepichka, F. Rosei, *Science* **2009**, *323*, 216-217.

[59] M. Johannes, S. Sofia, P. Maike, S. Jutta, H. Stefan, G. Leonhard, *J. Phys. Condens. Matter* **2012**, *24*, 394013.

[60] D. den Boer, M. Li, T. Habets, P. Iavicoli, A. E. Rowan, R. J. M. Nolte, S. Speller, D. B. Amabilino, S. De Feyter, J. A. A. W. Elemans, *Nat. Chem.* **2013**, *5*, 621.

[61] A. Ciesielski, S. Lena, S. Masiero, G. P. Spada, P. Samorì, *Angew. Chem. Int. Ed.* **2010**, *49*, 1963-1966.

[62] E. Ghijsens, O. Ivasenko, K. Tahara, H. Yamaga, S. Itano, T. Balandina, Y. Tobe, S. De Feyter, *ACS Nano* **2013**, *7*, 8031-8042.

[63] P. Samorì, K. Müllen, J. P. Rabe, *Adv. Mater.* **2004**, *16*, 1761-1765.

[64] R. Gutzler, T. Sirtl, J. F. Dienstmaier, K. Mahata, W. M. Heckl, M. Schmittel, M. Lackinger, *J. Am. Chem. Soc.* **2010**, *132*, 5084-5090.

[65] P. Vanoppen, P. C. M. Grim, M. Rucker, S. De Feyter, G. Moessner, S. Valiyaveettil, K. Müllen, F. C. De Schryver, *J Phys Chem-Us* **1996**, *100*, 19636-19641.

[66]    M. El Garah, E. Borré, A. Ciesielski, A. Dianat, R. Gutierrez, G. Cuniberti, S. Bellemin-Laponnaz, M. Mauro, P. Samorì, *Small* **2017**, *13*, 1701790.

[67]    M. El Garah, A. Ciesielski, N. Marets, V. Bulach, M. W. Hosseini, P. Samorì, *Chem. Commun.* **2014**, *50*, 12250-12253.

[68]    M. Surin, P. Samorì, A. Jouaiti, N. Kyritsakas, M. W. Hosseini, *Angew. Chem. Int. Ed.* **2007**, *46*, 245-249.

[69]    L. Piot, R. M. Meudtner, T. El Malah, S. Hecht, P. Samorì, *Chem-Eur J* **2009**, *15*, 4788-4792.

[70]    L. Piot, D. Bonifazi, P. Samorì, *Adv. Funct. Mater.* **2007**, *17*, 3689-3693.

[71]    A. Ciesielski, M. El Garah, S. Haar, P. Kovaříček, J.-M. Lehn, P. Samorì, *Nat. Chem.* **2014**, *6*, 1017-1023.

[72]    F. Schlütter, F. Rossel, M. Kivala, V. Enkelmann, J. P. Gisselbrecht, P. Ruffieux, R. Fasel, K. Müllen, *J. Am. Chem. Soc.* **2013**, *135*, 4550-4557.

[73]    S. Weigelt, C. Busse, C. Bombis, M. M. Knudsen, K. V. Gothelf, T. Strunskus, C. Woll, M. Dahlbom, B. Hammer, E. Laegsgaard, F. Besenbacher, T. R. Linderoth, *Angew. Chem. Int. Ed.* **2007**, *46*, 9227-9230.

[74]    Y. B. Li, J. H. Wan, K. Deng, X. N. Han, S. B. Lei, Y. L. Yang, Q. Y. Zheng, Q. D. Zeng, C. Wang, *J. Phys. Chem. C* **2011**, *115*, 6540-6544.

[75]    J. Plas, D. Waghray, J. Adisoejoso, O. Ivasenko, W. Dehaen, S. De Feyter, *Chem. Commun.* **2015**, *51*, 16338-16341.

[76]    F. Y. Hu, X. M. Zhang, X. C. Wang, S. Wang, H. Q. Wang, W. B. Duan, Q. D. Zeng, C. Wang, *ACS Appl. Mater. Interfaces* **2013**, *5*, 1583-1587.

[77]    J. Y. Yue, M. Markoulides, A. C. Regan, S. Y. Li, N. Chronakis, A. Gourdon, T. Chen, H. J. Yan, D. Wang, *Chem. Commun.* **2017**, *53*, 428-431.

[78]    J. Sun, Y. X. Yu, C. H. Liu, S. B. Lei, *J. Phys. Chem. C* **2017**, *121*, 3437-3444.

[79]    S. Weigelt, C. Busse, C. Bombis, M. M. Knudsen, K. V. Gothelf, E. Laegsgaard, F. Besenbacher, T. R. Linderoth, *Angew. Chem. Int. Ed.* **2008**, *47*, 4406-4410.

[80]    Y. X. Yu, J. B. Lin, S. B. Lei, *RSC Adv.* **2017**, *7*, 11496-11502.

[81]    Y. X. Yu, Y. L. Zheng, S. B. Lei, *J. Phys. Chem. C* **2017**, *121*, 593-599.

[82]    Y. X. Yu, J. Sun, S. B. Lei, *J. Phys. Chem. C* **2015**, *119*, 16777-16784.

[83]    M. Di Giovannantonio, T. Kosmala, B. Bonanni, G. Serrano, N. Zema, S. Turchini, D. Catone, K. Wandelt, D. Pasini, G. Contini, C. Goletti, *J. Phys. Chem. C* **2015**, *119*, 19228-19235.

[84]    R. Tanoue, R. Higuchi, K. Ikebe, S. Uemura, N. Kimizuka, A. Z. Stieg, J. K. Gimzewski, M. Kunitake, *Langmuir* **2012**, *28*, 13844-13851.

[85]    N. A. A. Zwaneveld, R. Pawlak, M. Abel, D. Catalin, D. Gigmes, D. Bertin, L. Porte, *J. Am. Chem. Soc.* **2008**, *130*, 6678-6679.

[86]    L. Lafferentz, V. Eberhardt, C. Dri, C. Africh, G. Comelli, F. Esch, S. Hecht, L. Grill, *Nat. Chem.* **2012**, *4*, 215-220.

[87]    J. Eichhorn, T. Strunskus, A. Rastgoo-Lahrood, D. Samanta, M. Schmittel, M. Lackinger, *Chem. Commun.* **2014**, *50*, 7680-7682.

[88]    R. Tanoue, R. Higuchi, N. Enoki, Y. Miyasato, S. Uemura, N. Kimizuka, A. Z. Stieg, J. K. Gimzewski, M. Kunitake, *ACS Nano* **2011**, *5*, 3923-3929.

[89]    X. H. Liu, C. Z. Guan, S. Y. Ding, W. Wang, H. J. Yan, D. Wang, L. J. Wan, *J. Am. Chem. Soc.* **2013**, *135*, 10470-10474.

[90]    M. O. Blunt, J. C. Russell, N. R. Champness, P. H. Beton, *Chem. Commun.* **2010**, *46*, 7157-7159.

[91]    L. R. Xu, X. Zhou, W. Q. Tian, T. Gao, Y. F. Zhang, S. B. Lei, Z. F. Liu, *Angew. Chem. Int. Ed.* **2014**, *53*, 9564-9568.

[92]    J. Sakamoto, J. van Heijst, O. Lukin, A. D. Schlüter, *Angew. Chem. Int. Ed.* **2009**, *48*, 1030-1069.

[93]    A. Thomas, *Angew. Chem. Int. Ed.* **2010**, *49*, 8328-8344.

[94]    Y. G. Zhang, S. N. Riduan, *Chem. Soc. Rev.* **2012**, *41*, 2083-2094.

[95]    P. Zhu, V. Meunier, *J. Chem. Phys.* **2012**, *137*, 16964-16970.

[96]     L. Cardenas, R. Gutzler, J. Lipton-Duffin, C. Y. Fu, J. L. Brusso, L. E. Dinca, M. Vondracak, Y. Fagot-Revurat, D. Malterre, F. Rosei, D. F. Perepichka, *Chem. Sci.* **2013**, *4*, 3263-3268.
[97]     R. Gutzler, D. F. Perepichka, *J. Am. Chem. Soc.* **2013**, *135*, 16585-16594.
[98]     N. R. Champness, *Nat. Nanotechnol.* **2007**, *2*, 671-672.
[99]     N. R. Champness, *Nat. Chem.* **2014**, *6*, 757-759.
[100]    S. Clair, O. Ourdjini, M. Abel, L. Porte, *Adv. Mater.* **2012**, *24*, 1252-1254.
[101]    S. Blankenburg, M. Bieri, R. Fasel, K. Mullen, C. A. Pignedoli, D. Passerone, *Small* **2010**, *6*, 2266-2271.
[102]    J. L. Yang, D. H. Yan, T. S. Jones, *Chem. Rev.* **2015**, *115*, 5570-5603.
[103]    J. Q. Liu, Z. Liu, C. J. Barrow, W. R. Yang, *Anal. Chim. Acta* **2015**, *859*, 1-19.
[104]    S. Nakagaki, G. K. B. Ferreira, G. M. Ucoski, K. Castro, *Molecules* **2013**, *18*, 7279-7308.
[105]    L. R. Xu, L. L. Cao, Z. X. Guo, Z. Q. Zha, S. B. Lei, *Chem. Commun.* **2015**, *51*, 8664-8667.
[106]    C. Z. Guan, D. Wang, L. J. Wan, *Chem. Commun.* **2012**, *48*, 2943-2945.
[107]    J. F. Dienstmaier, A. M. Gigler, A. J. Goetz, P. Knochel, T. Bein, A. Lyapin, S. Reichlmaier, W. M. Heckl, M. Lackinger, *ACS Nano* **2011**, *5*, 9737-9745.
[108]    J. F. Dienstmaier, D. D. Medina, M. Dogru, P. Knochel, T. Bein, W. M. Heckl, M. Lackinger, *ACS Nano* **2012**, *6*, 7234-7242.
[109]    Y. Hu, N. Goodeal, Y. Chen, A. M. Ganose, R. G. Palgrave, H. Bronstein, M. O. Blunt, *Chem. Commun.* **2016**, *52*, 9941-9944.
[110]    P. Bhyrappa, J. K. Young, J. S. Moore, K. S. Suslick, *J. Am. Chem. Soc.* **1996**, *118*, 5708-5711.
[111]    J. P. Collman, P. Denisevich, Y. Konai, M. Marrocco, C. Koval, F. C. Anson, *J. Am. Chem. Soc.* **1980**, *102*, 6027-6036.
[112]    A. Yella, H.-W. Lee, H. N. Tsao, C. Yi, A. K. Chandiran, M. K. Nazeeruddin, E. W.-G. Diau, C.-Y. Yeh, S. M. Zakeeruddin, M. Grätzel, *Science* **2011**, *334*, 629-634.
[113]    J. A. A. W. Elemans, R. van Hameren, R. J. M. Nolte, A. E. Rowan, *Adv. Mater.* **2006**, *18*, 1251-1266.
[114]    J. V. Barth, G. Costantini, K. Kern, *Nature* **2005**, *437*, 671-679.
[115]    S. Mohnani, D. Bonifazi, *Coord. Chem. Rev.* **2010**, *254*, 2342-2362.
[116]    W. Auwärter, D. Ecija, F. Klappenberger, J. V. Barth, *Nat. Chem.* **2015**, *7*, 105-120.
[117]    M. El Garah, N. Marets, M. Mauro, A. Aliprandi, S. Bonacchi, L. De Cola, A. Ciesielski, V. Bulach, M. W. Hosseini, P. Samorì, *J. Am. Chem. Soc.* **2015**, *137*, 8450-8459.
[118]    X. L. Sun, L. X. Fan, X. Zhou, W. Q. Tian, Z. X. Guo, Z. B. Li, X. K. Li, S. B. Lei, *Chem. Commun.* **2015**, *51*, 5864-5867.
[119]    S. Lei, K. Tahara, F. C. De Schryver, M. Van der Auweraer, Y. Tobe, S. De Feyter, *Angew. Chem. Int. Ed.* **2008**, *47*, 2964-2968.
[120]    L. Kampschulte, T. L. Werblowsky, R. S. K. Kishore, M. Schmittel, W. M. Heckl, M. Lackinger, *J. Am. Chem. Soc.* **2008**, *130*, 8502-8507.
[121]    C.-A. Palma, J. Bjork, M. Bonini, M. S. Dyer, A. Llanes-Pallas, D. Bonifazi, M. Persson, P. Samorì, *J. Am. Chem. Soc.* **2009**, *131*, 13062-13071.
[122]    A. Ciesielski, P. J. Szabelski, W. Rżysko, A. Cadeddu, T. R. Cook, P. J. Stang, P. Samorì, *J. Am. Chem. Soc.* **2013**, *135*, 6942-6950.
[123]    M. El Garah, A. Dianat, A. Cadeddu, R. Gutierrez, M. Cecchini, T. R. Cook, A. Ciesielski, P. J. Stang, G. Cuniberti, P. Samorì, *Small* **2016**, *12*, 343-350.
[124]    Y. Zhang, T. Gao, Y. Gao, S. Xie, Q. Ji, K. Yan, H. Peng, Z. Liu, *ACS Nano* **2011**, *5*, 4014-4022.
[125]    F. Banhart, J. Kotakoski, A. V. Krasheninnikov, *ACS Nano* **2011**, *5*, 26-41.